ASTRONOMY & ASTROPHYSICS
SUPPLEMENT SERIES

*Astron. Astrophys. Suppl. Ser.* **135**, 415–427 (1999)



# The limb flare of November 2, 1992: Physical conditions and scenario

**A.T. Altyntsev[1,⋆], V.V. Grechnev[1], H. Nakajima[2], K. Fujiki[2,⋆⋆], M. Nishio[2,⋆⋆⋆], and D.V. Prosovetsky[1]**

[1] Institute of Solar-Terrestrial Physics, Lermontov St. 126, Irkutsk 664033, Russia
e-mail: altyntsev@iszf.irk.ru; grechnev@iszf.irk.ru; proso@iszf.irk.ru
[2] Nobeyama Radio Observatory, NAOJ, Minamimaki, Minamisaku, Nagano 384-1305, Japan
e-mail: nakajima@nro.nao.ac.jp

Received June 15; accepted November 3, 1998

**Abstract.** The powerful X9 class flare was investigated using interferometric data of Nobeyama Radioheliograph (17 GHz) and SSRT (5.7 GHz). According to images obtained in circular polarization, it was found that the microwave burst was generated consequently in the sites, where opposite magnetic loops were in the close contact.

Steady exponential growth of the total microwave flux in the initial stage of the flare under significant reconstruction of the radio sources certifies that the development of the flare was conducted by some large-scale instability.

Radiation during the impulsive phase was produced by gyrosynchrotron emission of electrons trapped within a wide dome-like volume with $B \simeq 300$ G and $n \simeq 2\ 10^{10}$ cm$^{-3}$.

In the decay phase, the emission at higher frequencies was mainly produced by bremsstrahlung from high loops emitting soft X-rays. There is evidence of the energy release long after the impulsive phase: an intensive, rather compact microwave source in the locus of contact of two oppositely polarized regions in these loops and sub-bursts during 2 hours after the peak at low heights.

For the first time, a compact source of the sub-second pulses at 17 GHz was found to be located as high as $15\ 10^3$ km. They were due to gyrosynchrotron emission.

**Key words:** Sun: flares — magnetic fields — particle emission, radio radiation — X-rays

*Send offprint requests to*: A.T. Altyntsev

⋆ A.T. Altyntsev stayed at Nobeyama Radio Observatory as Foreign Research Fellow of National Astronomical Observatory.

⋆⋆ *Present address:* Solar-Terrestrial Environment Laboratory, Nagoya University, Toyokawa 442, Japan, e-mail: fujiki@stelab.nagoya-u.ac.jp

⋆⋆⋆ *Present address:* Department of physics, Kagoshima University, Kohrimoto, Kagoshima 890-0065, Japan, e-mail: nishio@sci.kagoshima-u.ac.jp

## 1. Introduction

There is a great interest to limb flares which show development of flares in height above the photosphere with emphasis of the coronal part of emission. An X9 class flare occurred on November 2, 1992 in the active region NOAA 7321 behind the western limb. It was a prominent Long-Duration Event at the decline of the 22$^{\rm nd}$ solar cycle: its decay lasted over 30 hours. The flare was recorded both by the Nobeyama Radioheliograph (NRH, 17 GHz) and the Siberian Solar Radio Telescope (SSRT, 5.7 GHz). The interest in this powerful flare is motivated, first, by the possibility to study microwave emission mechanisms which manifested themselves in extremely wide range of four orders of magnitude together with evolution of the spatial structure of microwave burst sources using two frequencies. Second, sub-second pulses were observed at both frequencies. So it is possible to estimate the heights above the photosphere and plasma parameters of sub-second pulse sources observed in this limb flare.

Some papers have been published devoted to study of different aspects of this flare: observations of sub-second microwave spikes at 5.7 GHz (Altyntsev et al. 1995); acceleration of high-energy electrons (Nakajima & Metcalf 1995); long-duration decay stage with large system of ascending $H_\alpha$ and soft X-ray (SXR) loops (Ichimoto et al. 1993; Feldman et al. 1995). The most powerful part of the impulsive phase of the flare was studied by Nakajima et al. (1998) using mainly hard X-ray *Yohkoh* and NRH data.

However, some aspects and features of the flare remain obscure. The overall scenario of the flare is still vague. The structure of the magnetic field and the physical conditions in the flaring plasma were not sufficiently investigated. These points constitute the main subject of the present paper.

Some specific issues we would like to address are as follows: observational material (Sect. 2), physical conditions derived from the observations (Sect. 3), the magnetic configuration and the proposed scenario for the flare (Sect. 4).

## 2. Observations

According to GOES data, the flare started at 02:30 (all times are given in UT). The latitude of flare site was 25°. The time interval of analysis is 00:23 − 06:00.

We used in this study primarily the following data.

- Radio maps of brightness temperature in intensity ($I$-images, $I = \frac{RCP+LCP}{2}$ with $RCP$ and $LCP$ being right- and left-handed circular polarization) and polarized emission ($V$-images, $V = \frac{RCP-LCP}{2}$) obtained at the NRH with 1 s temporal and $\sim 10''$ spatial resolution (Nakajima et al. 1994). Data of 50 ms time resolution was also available.
- A series of 1-dimensional spatial profiles of intensity and polarization distribution across the Sun (1-D scans) obtained at the SSRT with an interval of down to 56 ms (Smolkov et al. 1986; Altyntsev et al. 1994). The angular resolution of the SSRT varied during the flare from $15''$ to $22''$.
- Total flux time profiles at 3.75, 9.4, 17, and 35 GHz recorded at the polarimeters of Nobeyama Radio Observatory with the integration time of 0.3 s.
- Soft X-ray images obtained by the soft X-ray telescope onboard *Yohkoh* spacecraft (SXT; Tsuneta et al. 1991) after 03:05.

To avoid the influence of different spatial resolution, side lobes at 17 GHz, and saturation in some SSRT scans and soft X-ray images, we measured the height as a weighted centre of 1-D scans.

We must note that all estimates of height refer to the plane perpendicular to the line of sight. As the active region was already behind the limb, may be, all heights should be increased by $\leq 2.7\ 10^3$ km.

### 2.1. Development of the burst

Time profiles of flux at frequencies 3.75, 5.7, 9.4, 17, and 35 GHz are plotted in semi-logarithmic scale in Figs. 1a and 2. The flux density measured with the 35 GHz polarimeter is affected by the atmospheric absorption, so the flux density may be overestimated after 05:00.

The profile recorded at the SSRT (5.7 GHz) is not plotted around the peak of the burst since it is not reliable there due to multiple shifts of gain and presence of saturated records. Values of brightness temperature are available in NRH images. Peak brightness temperature was $1.2\ 10^9$ K at 17 GHz.

We can distinguish three main stages of the flare according to the behaviour of the microwave burst (Table 1). Before the rapid increase, flux at 5.7 and 9.4 GHz exceeded flux at other frequencies, and the spectral peak $\nu_{\rm peak}$ was lower than 10 GHz. Then, in the interval near the burst maximum, $\nu_{\rm peak}$ was between 17 and 35 GHz. During the rapid decrease of the flux $\nu_{\rm peak}$ shifted again to a frequency of lower than 17 GHz. In the long-duration decay phase (after 03:22), the spectral index changed its sign again, and the relative value of flux increased with frequency. An exception – the interval during the sub-burst of 04:08 − 04:12 when the peak frequency was about 4 GHz.

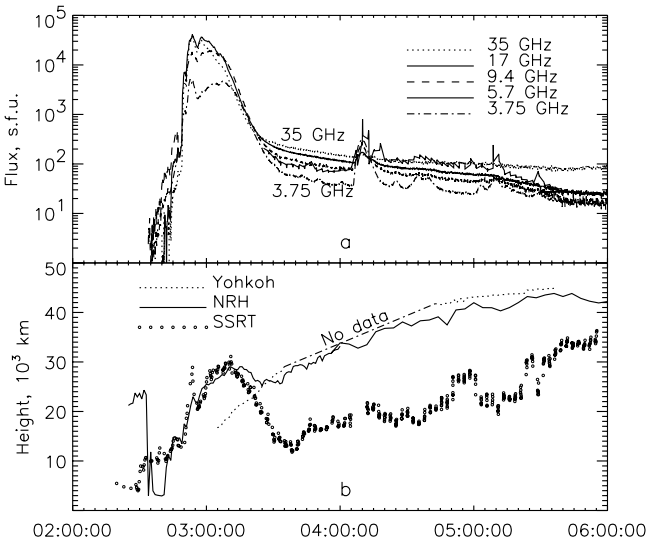


**Fig. 1.** Microwave time profiles: **a)** total flux at different frequencies and maximum of brightness temperature at 17 GHz; **b)** effective height according to microwaves and *Yohkoh*/SXT data

Variations of the height of microwave and soft X-ray sources above the limb are shown in Fig. 1b. Large height of the emitting region at 17 GHz before the flare is explained by the fact that this region was amorphous and extended up to significant heights without prominent brightness centres. When the flare started, two microwave sources became prominent: one close to the optical limb (17 GHz) and another one – at a height of about $10\ 10^3$ km (5.7 GHz). Later the relative brightness of the upper source increased, and this source began to be dominant at both frequencies.

Further, during more than two hours, a rising motion of the 17 GHz source was observed with the average velocity of about 3 km s$^{-1}$. Two intervals were outstanding: one during sharp rise of flux, when the velocity reached 15 km s$^{-1}$, and another one (03:16 − 03:22), during which the sources' height slightly decreased.

Variations of the height at 5.7 GHz during the first two stages were similar to that ones at 17 GHz. Near the peak of the burst, the low-frequency source was mainly higher. After that, the source at 5.7 GHz descended. In the decay phase, the weighted height of the sources at 5.7 GHz increased similarly to the height of 17 GHz ones, but it was about $15\ 10^3$ km less.

The soft X-ray source was located lower than the microwave (17 GHz) one during the impulsive phase, and close to it in the decay phase after 03:22.

Let us consider the stages of the flare in detail.

**Table 1.** The stages of the flare

| UT | Characterisation | Flux (s.f.u.) | $\nu_{\rm peak}$ (GHz) | Height ($10^3$ km) | Emission mechanism |
|---|---|---|---|---|---|
| *before* 02:30 | pre-flare stage: approach of oppositely-polarized regions | $< 5$ | | | free-free |
| $1^{\rm st}$ **stage** — Rise of radio flux | | | | | |
| 02:30 − 02:49 | exponential growth, $\tau \simeq 160$ s | $5 - 100$ | $< 10$ | $3 - 15$ | gyrosynchrotron |
| 02:44 − 02:46 | sub-second pulses at 17 GHz, $\tau < 1$ s | $< 10$ | $< 10$ | 15 | gyrosynchrotron |
| 02:49 − 02:54 | impulsive rise, $\tau \simeq 10$ s | $10^2 - 4\ 10^4$ | $17 < \nu_{\rm peak} < 35$ | $15 - 25$ | gyrosynchrotron |
| 02:53 − 02:55 | spikes at 5.7 GHz, $\tau \leq 0.1$ s | $\sim 10^3$ | 5.7 | $\simeq 30$ | plasma |
| 02:54 | peak of the burst at 17 GHz, the dome-like source began to grow | $4\ 10^4$ | $17 < \nu_{\rm peak} < 35$ | 23 (17 GHz) | gyrosynchrotron |
| 02:58 | $2^{\rm nd}$ peak at 17 GHz | $2\ 10^4$ | $17 < \nu_{\rm peak} < 35$ | 25 (17 GHz) | gyrosynchrotron |
| $2^{\rm nd}$ **stage** — Relatively fast decrease of the flux | | | | | gyrosynchrotron |
| 02:59 − 03:10 | decrease with $\tau = 10$ min | $2\ 10^4 - 1\ 10^4$ | spectrum shifted leftwards | $25 - 29$ | |
| 03:10 − 03:12 | stop of the growth of the area, disappearance of the upper 5.7 GHz source | $1\ 10^4 - 4\ 10^3$ | | 29 | |
| 03:12 − 03:23 | decrease with $\tau = 4.1$ min | $4\ 10^3 - 500$ | $\sim 10$ | $29 - 26$ | |
| $3^{\rm rd}$ **stage** — Long-duration decay | | | | | |
| 03:23 − 06:00 | slow decay of the upper source, $\tau \sim 60$ min | $500 - 20$ | $> 35$ | $26 - 45$ | free-free |
| 03:40 − 05:40 | series of sub-bursts | $< 150$ | $\simeq 4$ | | gyrosynchrotron |
| 04:08 − 04:12 | most powerful sub-burst | 350 (5.7 GHz) | $\simeq 4$ | | gyrosynchrotron |

2.1.1. The first stage

Figure 2 shows expanded time profiles of total flux at different frequencies and the maximum of brightness temperature ($T_B$) at 17 GHz. It is remarkable that, on the average, the time profile of flux followed closely the exponential shape $\exp\left(\frac{t-t_0}{\tau}\right)$ during the first 17 minutes. For the flux $\tau \simeq 160$ s, so this interval exceeded $5\tau$.

At 17 GHz, $\tau \simeq 200$ s for the maximum of $T_B$ and the origin $t_0$ corresponds to 01:55. Note that before 01:50 the maximum of the brightness temperature within the flaring region decreased. It suggests that the real onset of the flare started at 01:55 indeed.

Growth rate of microwave emission after 02:48:53 went sharply up and both $T_B$ and the flux increased in an order of magnitude within one minute at all the considered frequencies. The largest increase was observed at higher frequencies. After that, time profiles at 9.4 and 17 GHz became smoother.

Fine time structures were observed at all the frequencies on the background of the exponential growth. The shortest structures detected at 17 GHz in the records with 50 ms resolution were two similar prominent series of subsecond pulses around 02:44:50 and 02:45:10.

The first set (Fig. 3, trends subtracted) consists of two rapidly damped pulses with duration of $\simeq 0.5$ s. Corresponding enhancement of flux was also observed at 5.7 and 9.4 GHz. The pulses were weakly positively polarized (some percent) and were well above the noise level. The decline was steep ($< 0.5$ s), but its start was delayed

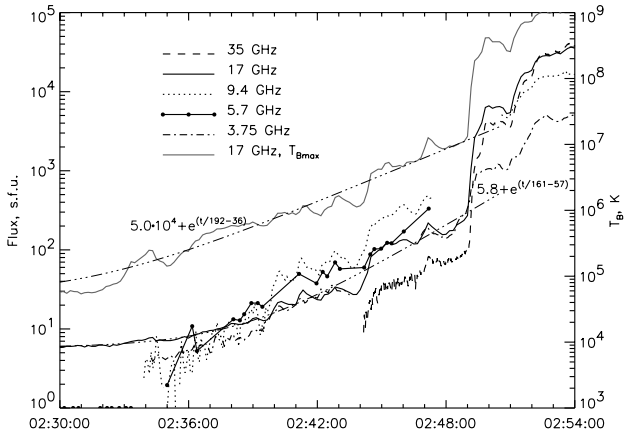


**Fig. 2.** Extended time profiles of the total flux at different frequencies and the brightness temperature at 17 GHz in the initial stage

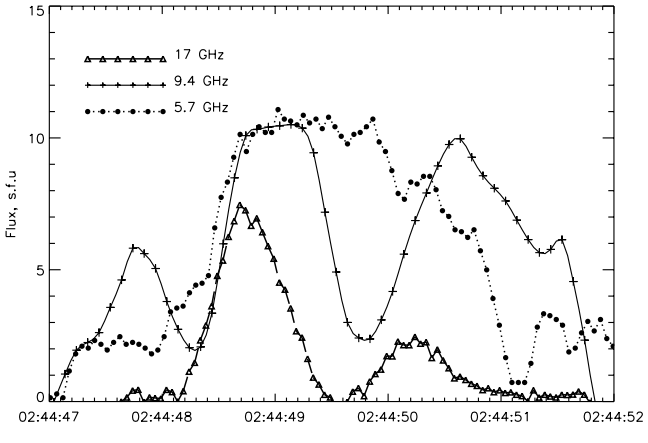


**Fig. 3.** Fine temporal structure at different frequencies. Time resolution is 50 ms at 17 GHz, 56 ms at 5.7 GHz, 0.1 s at 9.4 GHz. The record of 9.4 GHz was averaged over 0.3 s

at the lower frequencies. The second set was similar to the first one, but at 5.7 GHz record it could not be detected above the noise level.

A series of sub-second pulses (spikes) observed at the end of this stage in SSRT 1-D scans since 02:53:45 to 02:54:45 was described by Altyntsev et al. (1995). The minimal duration of those spikes was less than the temporal resolution of the receiver (56 ms) and the maximal one was about 100 ms. Their flux ranged from 700 up to 1800 s.f.u. In this case, no corresponding pulses exceeding noise level were detected at the other frequencies.

Let us consider relation between features in time profile and changes in spatial structure of the emitting region observed at 17 GHz (Fig. 4). Frames of the upper row correspond to the phase of exponential growth. It is remarkable that the structure of microwave sources varied considerably during the steady exponential growth of both $T_B$ and flux.

In the frame of 02:37:00, the only compact positively-polarized (up to 38%) source (1) was seen, and it was located close to the limb. Later the region of increased emission expanded along the limb to the north. Another positively-polarized source (2) appeared in the northern direction at 02:39:50 also close to the limb. Its polarization was up to 20%. At 02:40:00, the third source (3) emerged above the second one at a height of 15 $10^3$ km (the frame of 02:43:50). This source had relatively low ($\sim 5\%$) positive polarization ($RCP$).

Time profiles of brightness temperature for the three low-lying sources observed during the exponential growth are given in Fig. 5. The bottom of the figure is the result of subtraction of the exponential trends from each of the curves. We can see that the time profiles of the sources 2 and 3 are very close, and the profile of the source 1 differs significantly from them. The sources 2 and 3 were located radially with a distance between them of 14 $10^3$ km. From the bottom of this figure we can see similar oscillations of the brightness temperature with a period of 70 s occurred in these sources. There is a delay of peaks in the source 3 with respect to the source 2 by $\simeq$ 6.6 s. If these sources corresponded to the same loop, then the delay may be due to difference of trapping time in these sources. It also can be explained by motion of some exciting agent from below with a velocity of $\geq 2\ 10^3$ km s$^{-1}$. Another geometry was also possible. The sources 2 and 3 may correspond to different loops intercrossing and interacting behind the limb.

The increase of flux in the interval 02:44:00 − 02:44:30 was connected with appearance of a new positively polarized source at the same height as the source 3 towards south-east (Fig. 4, the upper right frame). The brightness centre in $I$-images moved in the southern direction, to a position between the regions of opposite polarization. Note, that both sets of sub-second pulses occurred at 17 GHz were located in this brightness centre (15 $10^3$ km above the limb). Sizes of their sources were close to the beam size of NRH (7 thousand km ×10 thousand km).

The sharp increase of $T_B$ and flux at the end of the first stage corresponds to a fast extension of an $RCP$ source pressed to the negatively polarized region from below (02:49:50). Starting from this time, the source in $I$-image became dome-like with the lower edge located $\simeq$ 15 $10^3$ km above the optical limb. This emitting region rapidly expanded to the south-west direction and then varied negligibly till 03:20. The peaks at 02:53:55 and 02:58:50 were associated with reconstruction of the $LCP$-source and enlargement of the nearest part of the $RCP$-source (see Fig. 4, 02:53:50). The degree of * polarization did not exceed 20% for these sources.

To compare structures visible in 2-D images at 17 GHz and 1-D scans at 5.7 GHz, let us consider the Figs. 1b and 6. During the first stage of the flare, the height of the sources above the limb increased at both 17 and 5.7 GHz.

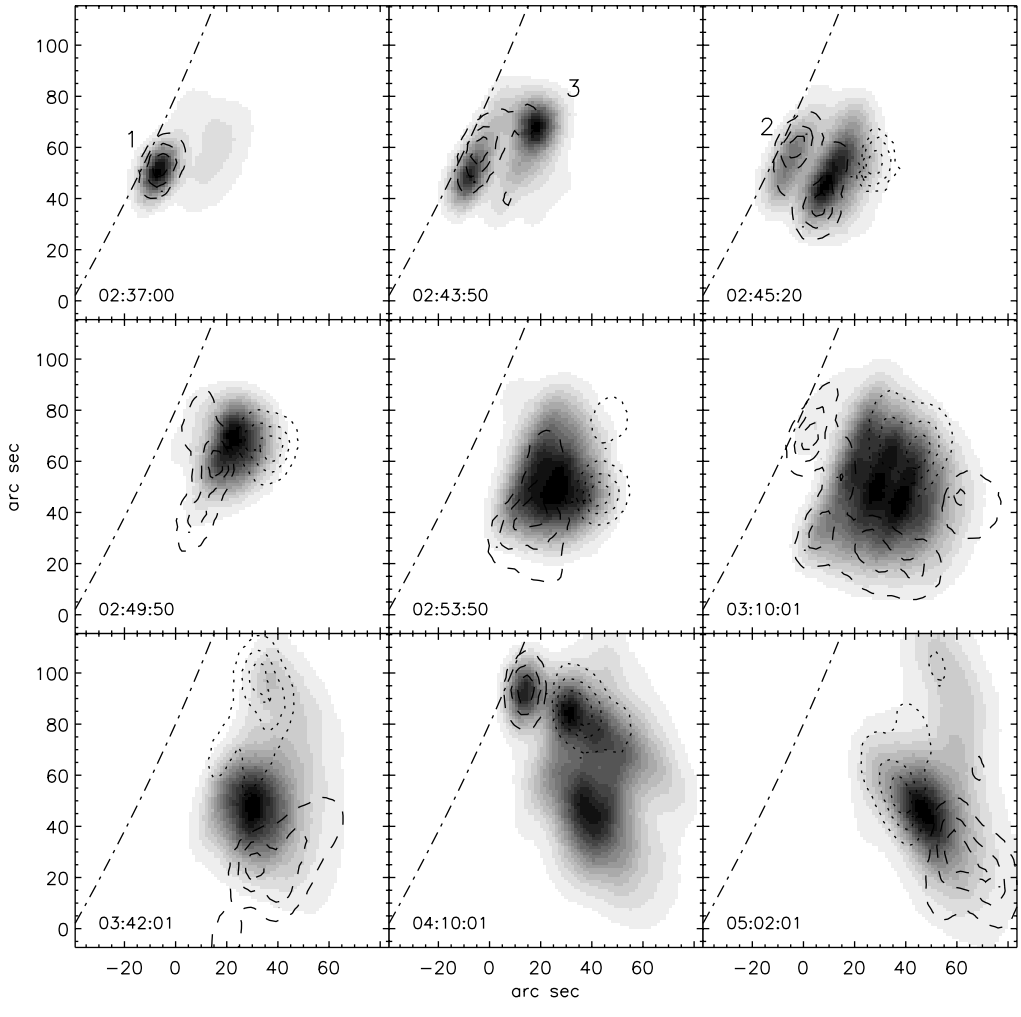


**Fig. 4.** Structure of microwave sources in intensity and polarization observed at 17 GHz. Dashed lines – $RCP$, dotted – $LCP$. Three first sources are marked by digits in the upper row. Contour levels are $(0.2, 0.5, 0.8)$ of the maximum of each polarity. The north is up

The sources were close till the sharp rise of flux (Fig. 6, 02:45:00). A short-duration increase of the height prominent at 5.7 GHz and faint at 17 GHz occurred at 02:54. The brightness centre at 5.7 GHz became 10 $10^3$ km higher than the 17 GHz source at this time. It indicates appearance of a new source which contributed considerably to the total flux at 5.7 GHz, but was not seen at 17 GHz. Note that the source of 5.7 GHz sub-second spikes coincided with the brightest point of the background burst at this frequency, i.e. with the source located above the region emitting at 17 GHz.

### 2.1.2. The second stage

During this stage, the flux at 17 GHz decreased in about two orders of magnitude. At first, the flux declined till 03:09 with a time scale of $\tau = 10$ min. After that, the decrease quickened more than two times ($\tau = 4.1$ min). The source seen in $I$-images had a dome-like shape and varied slowly during this stage. The area of the source gradually grew till 03:10 when its size reached $\simeq 37''$ and then became constant. Extended polarized sources encircled this source (Fig. 4).

Increasing of the flux continued at lower frequencies. At 5.7 GHz, this increase was due to appearance once more of the higher source invisible at 17 GHz (Figs. 1b and 6). Its height was close to that one at 02:54. This source disappeared near 03:10 when the decay at 17 GHz was accelerated.

After 03:00, *Yohkoh* data is available. At 03:00, a compact hard X-ray source was observed whose height 34 $10^3$ km (Nakajima et al. 1998) was close to the height of the upper source at 5.7 GHz. The soft X-ray source was significantly lower than the microwave sources at both frequencies and the HXT one at this time. The height of the soft X-ray source above the limb was increasing, and in the end of the second stage, the heights of the microwave sources and the soft X-ray kernel became close.

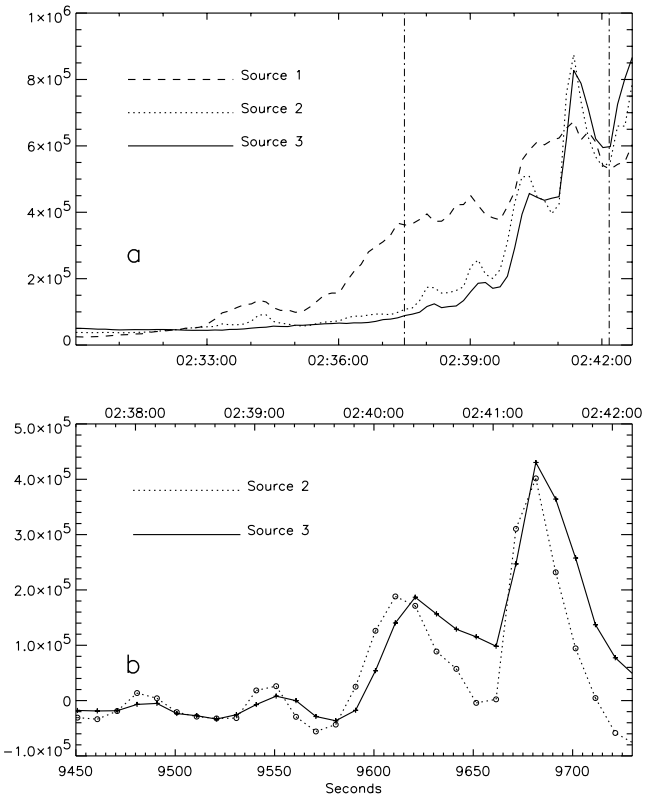


**Fig. 5. a)** Oscillatory initial part of the time profiles of brightness temperature in three low-lying sources; **b)** expanded time profiles of the sources 2 and 3 with subtracted exponential trend. The time interval of the lower plot is marked in the upper one by vertical lines

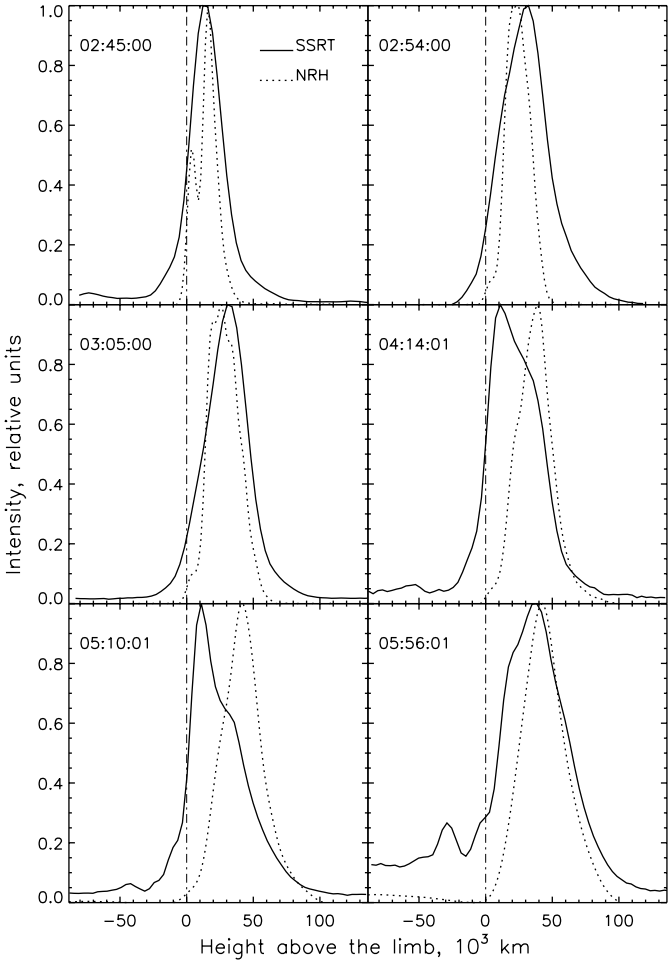


**Fig. 6.** A set of 1-dimensional scans obtained at the SSRT and computed from images obtained at the NRH during the flare

### 2.1.3. The third stage

It lasted until the end of the observations. The behaviour of the burst at 17 and 35 GHz was characterised by large time scales of variations (except for rather faint subbursts). Note also that the time profiles at lower frequencies were not smooth: a series of sub-bursts during two hours is detectable in semi-logarithmic profiles at 3.75 and 5.7 GHz. Corresponding enhancement was observed at 17 and 35 GHz only for the most powerful sub-burst (04:12). Microwave emission of at least two components was obviously present within the interval 04:08 − 05:40, i.e. slow decay of high-frequency residual emission of the upper source, and weaker low-frequency sub-burst emission of the lower sources.

The upper source at 17 GHz shifted above the $LCP$-region and moved upwards extending to the north (Fig. 4, the bottom row). Polarization was small, but, as before, the marked brightness centre in $I$-images was situated between the regions of opposite polarization. The brightness centres in soft X-rays and in 17 GHz image became close in this stage. The lower source can be seen in 17 GHz map during the relatively short interval near 04:10 (Fig. 4). In Fig. 7a, the difference of two images obtained at 04:10 and 04:08 is shown. We investigated time profiles of $T_B$ in different points of the image. No direct relation between the lower impulsive and the upper quasi-stationary sources was found: the impulsive increase of the brightness temperature in the lower source had no response in the upper one, although it marked a loop enveloping the upper source. The impulsive brightening in the enveloping loop was delayed with respect to the lower source. It may be interpreted as trapping of the electrons in the upper part of the loop with $\sim$100 s.

The behaviour of the effective source's height at 5.7 GHz (Fig. 1b) is due to variations of relative brightness of two sources separated in height. They can be distinguished in SSRT 1-D scans in the interval 04:12:51 − 05:54:49 (Fig. 6). The lower source had a height of $\simeq 10\ 10^3$ km and the upper one moved upward together with the 17 GHz source. The degree of polarization at 04:10 was 29% for the lower $RCP$-source, and 13% for the $LCP$-region.

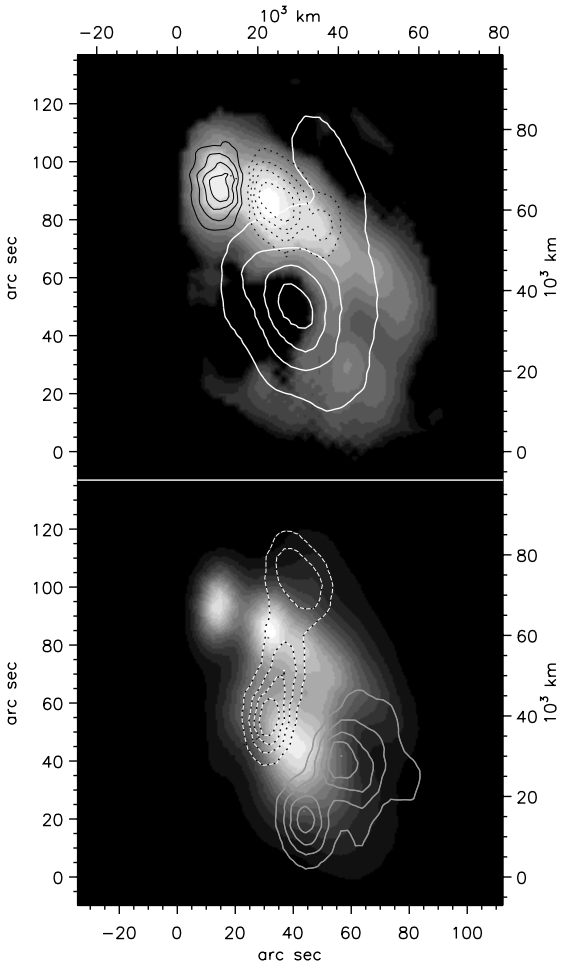


**Fig. 7.** The loop appeared during the sub-burst at 04:10 UT: **a)** colour – difference of $I$-images of 04:10 and 04:08, black contours – difference of $V$-images of 04:10 and 04:08, white contours – $I$-image of 04:06. **b)** colour – $I$-image of 04:10, contours – $V$-image of 04:06. Broken lines – negative polarization. To reveal the whole shape of the loop visible in the subtracted $I$-image, non-linear display was applied. Contour levels of polarization are $(0.2, 0.4, 0.6, 0.8)$ of the maximum of each polarity ($-10\%$ and $+25\%$). Contour levels of $I$-image of 04:06 are $(0.5, 1.5, 2.5, 3.5)\,10^6$ K

2.1.4. Summary of the development of the spatial structure

A region of enhanced microwave emission was observed a few hours before the flare high in the corona, where the flaring sources appeared later. Extended weakly polarized regions existed on the periphery of this wide area. The positive ones were lower, close to the optical limb. In the first three pictures (Fig. 8), two oppositely-polarized regions moved towards each other. This motion indicates movement of components of the magnetic structure, and also suggests a shear motion at footpoints of magnetic loops. The structure of the polarized region in the last picture became similar to that observed at the beginning of the flare. The degree of polarization did not exceed 10%.

Generalised pictures of the flare development are shown in Fig. 9. These pictures were obtained by addition of all the frames, each of which was previously normalised to unit.

Low-lying sources with high degree of polarization were observed in the beginning of the flare. During the first stage, sources in $I$-images (Fig. 9a) moving towards north-west got the dome-like shape and then enlarged towards south-west. In the second stage, when the intensity decreased, the shape and the size of the microwave source were not changed considerably. In the third (last) stage, the source in $I$-images expanded slowly and moved towards north-west. Note that sometimes in this stage also a source located close to the optical limb was observed.

More complicated structure is seen in the $V$-map averaged during the flare (Fig. 9b). $RCP$-sources appeared one by one around the $LCP$-sources. This large-scale structure as a whole did not change itself significantly during the flare, and its parts came subsequently in sight.

Consequently, the main structural components of the area emitted in microwaves before and during the flare were large-scale systems of intercrossed magnetic ropes. Cross sections of, at least, three of them were seen in polarization structure. The first system was represented by the low-lying strongly polarized $RCP$ sources which corresponded to the top parts of low loops. The other two large-scale systems were represented by the regions of weak opposite polarization which were seen high in the corona in the main impulsive phase (in the late first and second stage) and in the third stage. In general, the situation can be characterised as a multi-level and a multi-loop one both at the onset and in the end of the flare.

## 3. Estimates of physical parameters

### *3.1. Plasma parameters*

3.1.1. Magnetic field

The general structure of magnetic field before the flare can be seen in Fig. 8. Fujiki (1997) has shown that the pre-flare emission at 17 GHz for the series of flares including the event of November 2, 1992 was optically thin and had free-free origin. The observed averaged degree of polarization ($\simeq 5\%$) leads us to an estimate of the line-of-sight component of magnetic field $B_\mathrm{l} \simeq 150$ G.

At 03:07, a bright SXR kernel was located inside the dome-shaped microwave source. In the bright SXR kernel, plasma density was $n \leq 4\,10^{11}$ cm$^{-3}$, and temperature was $1.4\ 10^7$ K (Feldman et al. 1995). Demand for magnetic pressure to exceed the plasma one leads us to a limitation of $B \geq 200$ G in the SXR kernel in the second stage of the flare.

We assume that the emission of the burst around the peak had gyrosynchrotron origin as it is usual for this

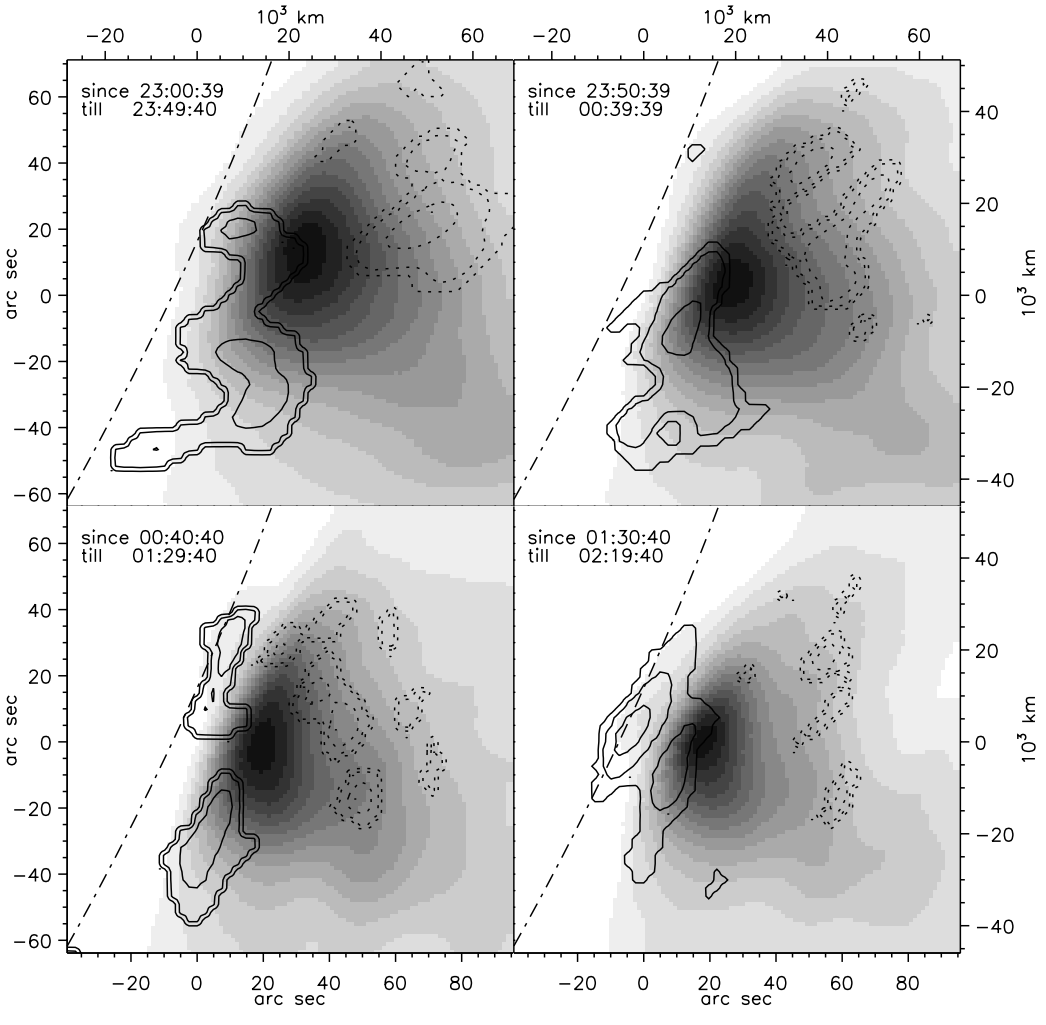


**Fig. 8.** The structure of microwave sources in intensity ($I$; colour) and polarization ($V$; contours, dotted are negative) before the flare. Each frame was averaged over 49 minutes. Contour levels are $(0.2, 0.5, 0.8)$ of the maximum of each polarity

spectral range. The power-law spectral index at 02:57:25 obtained from data of 35 and 80 GHz radiometers of Nobeyama Radio Observatory, was 1.5, and the power-law index of the electron spectrum, was 3. Fit of the microwave spectra with the help of Ramaty's code (Ramaty 1969; Ramaty et al. 1994) shows that the magnetic field of 200 G is rather low to fit the turnover frequency of more than 17 GHz. Sufficiently good fit of the total flux data can be achieved with $B = 300 - 800$ G (Nakajima & Metcalf 1995).

Low degree of polarization of the 17 GHz source (as a rule, less than 10%) near the peak of the burst shows that the magnetic field did not exceed a few hundred gauss. Hence we believe that the value of the magnetic field was about the lower boundary of this range (300 G).

3.1.2. Density of background plasma

The observed spectra do not reveal any marks of suppression of emissivity at frequencies down to 3.75 GHz. So we can obtain the upper limit of the background plasma density in the main microwave source assuming that the Razin-Tsytovich frequency $\nu = \frac{\nu_p^2}{\nu_B}$ was less than 3.75 GHz. This upper limit equals to 4 $10^{10}$ cm$^{-3}$.

Another estimate of the background plasma density can be obtained from the decay time of the emission at 17 GHz (4.1 min) within the interval 03:12 − 03:22. As we will show below, the bulk of emitting electrons had the energy of about $\mathcal{E} \sim 2$ MeV in this time interval. We assume that the decay time was equal to the life time of electrons. We can estimate the energy loss time from the expression (Bai & Ramaty 1976)
$T_{\rm loss} = 2.6\ 10^9\, \mathcal{E}/n$.

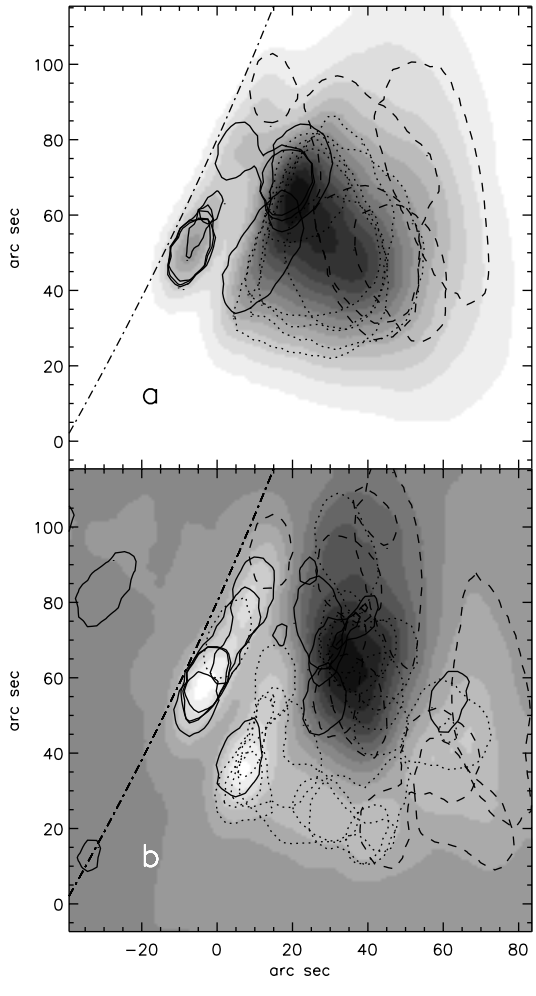


**Fig. 9.** The maps averaged over the whole sets of 17 GHz maps in intensity ($I$; **a)** and polarization ($V$; **b)** obtained during the flare are shown by colour. Half-height contours of the sources in $I$- and $V$-images are shown for some instants. Three different stages of the burst are marked by different line styles: solid – the 1st stage, dotted – the 2nd stage, dashed – the 3rd stage

Then the background plasma density was $n = 2.1\,10^{10}\,\mathrm{cm}^{-3}$ which is in accordance with the estimate from the Razin-Tsytovich effect.

3.1.3. Emitting electrons

To analyse parameters of emitting electrons, we used Ramaty's code (Ramaty et al. 1994) for modelling of gyrosynchrotron emission. Changing the energy boundaries of electron distribution and correlating the calculated spectrum with the observational data, we estimated the energy range of electrons that radiated the bulk of the observed microwave emission.

The turnover frequency during the exponential growth was about 9 GHz, and the flux before the rapid rise (at 02:47) was 450 s.f.u. at 9.4 GHz and 58 s.f.u. at 35 GHz. So the spectral slope was the same as that around the peaks which were considered above, and then the spectral index of electrons was equal to 3. For the size of the upper source of $\simeq 20''$ and the magnetic field of 300 G, the Ramaty's code gave the estimate of the distribution of non-thermal electrons as $\mathrm{d}N/\mathrm{d}\mathcal{E} = 1.3\ 10^{30}\,\mathcal{E}^{-3}\ \mathrm{MeV}^{-1}$. The main contribution to the observed microwave emission was given by electrons with energy in the range of $0.1 - 3$ MeV.

The modelling of the electron distribution in the main dome-like source in the second stage (source size $37''$) showed that the shift of the turnover frequency to a value above 17 GHz was connected with the increase of $\mathrm{d}N/\mathrm{d}\mathcal{E}$ by more than two orders of magnitude in the energy range of $0.5 - 5$ MeV. This source became optically thick for the emission of 5.7 GHz.

The upper source above the dome-like one was observed clearly in 1d-scans at 5.7 GHz during the interval with spikes recorded by SSRT. The turnover frequency in this source was considerably less than 17 GHz, and the number of high-energy electrons in it must be considerably less than that number in the main dome-like source.

In the last stage, the main sources at 5.7 GHz and at 17 GHz differed essentially in time profiles, emission spectrum and height.

The main source at 5.7 GHz was located at a height of about $10\ 10^3$ km. At the frequencies below 9.4 GHz, it manifested itself in a series of sub-bursts with a magnitude of tens s.f.u. occurred till 05:40. The spectra had a turnover frequency of $\leq 3.75$ GHz. This source had a gyrosynchrotron origin. It appeared at 17 GHz during the most powerful sub-burst at 04:12 as a radially elongated source.

The main 17 GHz source was close to the soft X-ray one in the decay phase. The values of the flux increased with frequency, which points to free-free emission mechanism. The brightness temperature was $(3 - 5)\ 10^6$ K at 17 GHz. Plasma parameters in the emitting SXR region were estimated by Ichimoto et al. (1993) and Feldman et al. (1995) from *Yohkoh*/SXT data. They have obtained for the bright kernel a temperature of $10^7$ K, a density of $10^{11}$ cm$^{-3}$, and a size of $10^9$ cm. The corresponding calculated value of the brightness temperature for free-free emission, $T_B = 3\ 10^6$ K, agrees with the observed one.

*3.2. Sub-second pulses*

For the first time, we have found a 17 GHz source of sub-second pulses to be located well above the photosphere. The source size $< 7\ 10^3$ km. The time profiles of the observed sub-second pulses show simultaneous onset at the lower frequencies. Assuming that the duration of signal's rise (0.6 s) was equal to the propagation time with Alfvèn velocity ($4.6\ 10^8$ cm s$^{-1}$ using the ambient density of $2.1\ 10^{10}$ cm$^{-3}$ and the magnetic field of 300 G) across

the region of energy release, we obtain that its size was about 2.8 $10^3$ km. This estimate does not contradict the apparent size of the microwave source.

The microwave spectrum had a maximum in the frequency interval of $5.7 - 9$ GHz. The degree of polarization for the pulses was a few percent. The simultaneous enhancement of the total flux at $5.7 - 17$ GHz can be interpreted in terms of gyrosynchrotron emission of nonthermal electrons. At the peak of the pulse, the power-law index estimated from the ratio of the flux at 9.4 and 17 GHz, was about 2, and the electron spectrum was harder than that one of the background burst.

For the source size of 2.8 $10^3$ km and the magnetic field of 300 G, the observed microwave flux corresponded to a small density fraction of accelerated electrons with $\mathrm{d}N/\mathrm{d}\mathcal{E} = 5\ 10^{28}\,\mathcal{E}^{-2}$ MeV$^{-1}$. To emit the observed flux at 17 GHz, the upper cutoff energy of the electron spectrum must be $\geq 2$ MeV. With the typical energy of radiating electrons of $1-2$ MeV, the observed duration of the decay at this frequency was much less than the life time due to Coulomb collisions ($\sim 10^2$ s using the ambient density of 2.1 $10^{10}$ cm$^{-3}$). Since the observations suggest that the electrons were accelerated and confined in a small region high in the corona, these processes were controlled not by Coulomb collisions, but by other mechanisms such as some plasma turbulence. This fine time structure may be indeed a manifestation of a fragmented energy release in a flaring site (see, e.g., Benz 1986).

Another situation was for sub-second pulses at 5.7 GHz occurred in the source above the dome-like one. There was no corresponding brightening at the other frequencies, so the bandwidth of the emission must be rather narrow. A detailed description of these pulses was made by Altyntsev et al. (1995). The size of the source of these pulses appeared to be $\simeq 50''$. It was found that the apparent size of the source was affected by a significant scattering of the microwave emission at this frequency due to turbulent inhomogeneities of plasma density. (It certainly could affect the observed sources at 5.7 GHz.) From the low degree of the observed polarization and rather high magnetic field needed for electron cyclotron maser mechanism, a conclusion was made that a plasma emission mechanism is favourable. In this case plasma density in the source must exceed $10^{11}$ cm$^{-3}$.

From the study of similar pulses observed during the flare of September 6, 1992 occurred on the solar disk (Altyntsev et al. 1998), it has been shown that the source was projected onto a loop emitting soft X-rays with sufficiently high density. In the limb flare of November 2, 1992, we see that the dense SXR loop-top was located inside the optically thick dome-like source, and the sub-second impulsive source was much higher. The estimate of plasma density in the dome-like source was $\sim 2.1\ 10^{10}$ cm$^{-3}$. If the plasma density in the surroundings of the impulsive source was of the same order, then, to realize the density of $\geq 10^{11}$ cm$^{-3}$, the background plasma in the impulsive source must be compressed a few times. Such a compression is reasonable for a reconnection site, where the energy release occurred.

## 4. An interpretation of the flare

### *4.1. Magnetic configuration*

The magnetic structure of the flare region can be derived from the polarization structure in microwaves (see Fig. 9b). The observations of the present event suggest that the main structural components were large-scale systems of intercrossed magnetic ropes during the whole development of the flare, as described in the Sect. 2.1.4.

Figures 10 and 11 show an illustration of a possible magnetic configuration in this event. In Figs. 10a–c, diagrams of the most significant magnetic structures in the three stages of the flare are presented. The orientation of these schemes is the same as that one in Fig. 4. Figure 11a shows a sketch of a possible spatial configuration of some foremost loops to give a conception of their disposition. Figure 11b is an $H_\alpha$ image of post-flare loops to compare it with that sketch. The orientation of the sketch in Fig. 11a is chosen to show the entire loops whose parts were in fact hidden behind the limb. The orientation of the $H_\alpha$ image in Fig. 11b is chosen to match the sketch.

In the beginning of the first stage (Fig. 10a), the low-lying sources located near the limb represented closeness of the brightness centres in $I$- and $V$-images. High degree of their polarization (up to 38%) indicated orientation of the corresponding magnetic loops close to the line of sight. These loops represented the low-lying magnetic system whose most part was hidden by the limb.

Further, sources appeared higher. A bipolar structure in polarization became typical late in the first stage and the second stage. A possible magnetic configuration seems to be two intercrossed magnetic ropes as shown in Fig. 10b. In this configuration, energy release is caused by magnetic reconnection between the two ropes.

In a reconnection of the two original magnetic ropes, two new sets of loops must be created: short loops, descending from the reconnection site, and long ones, slowly expanding upwards, which were braided within the original ropes. The shape of the short loops was closer to the circular one which was seen as the dome-like source. Cross sections of the long loops were seen in polarization. After the reconnection, the long loops did not change their orientation drastically, and the polarized emission which escaped from them delineated the magnetic structure.

The magnetic tension tended to lift reconnected long loops which could force the interaction between the original ropes in the first stage of the flare. Their upward motion can explain the gradual growth upwards of energy release sites and the appearance of the upper microwave source coincided with the hard X-ray one at the

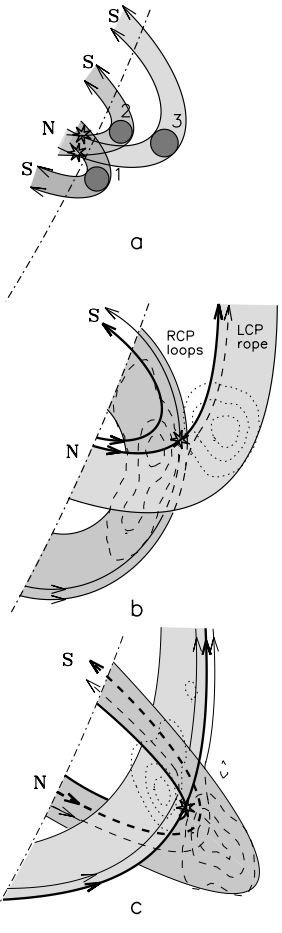


**Fig. 10.** Schemes of the most significant magnetic structures in the three stages of the flare. Reconnection sites are marked by stars. Some of magnetic loops are shown schematically by lines with arrows indicating direction of the magnetic field. The parts of loops which were not hidden by overlain ones are plotted by solid lines. Those parts of loops which could not be seen because of overlain loops are plotted by broken lines. Dotted and dashed closed contours reproduce the polarization observed in microwaves (see Fig. 4). **a)** the 1st stage, the sources 1, 2, and 3. The $N$ polarity region is located farther behind the limb than the $S$ polarity footpoints. The region of interaction (marked by stars) is also behind the limb. **b)** the 2nd stage, 02:49:50 UT. Rapid increase of energy release. **c)** the 3rd stage, 05:02:01 UT

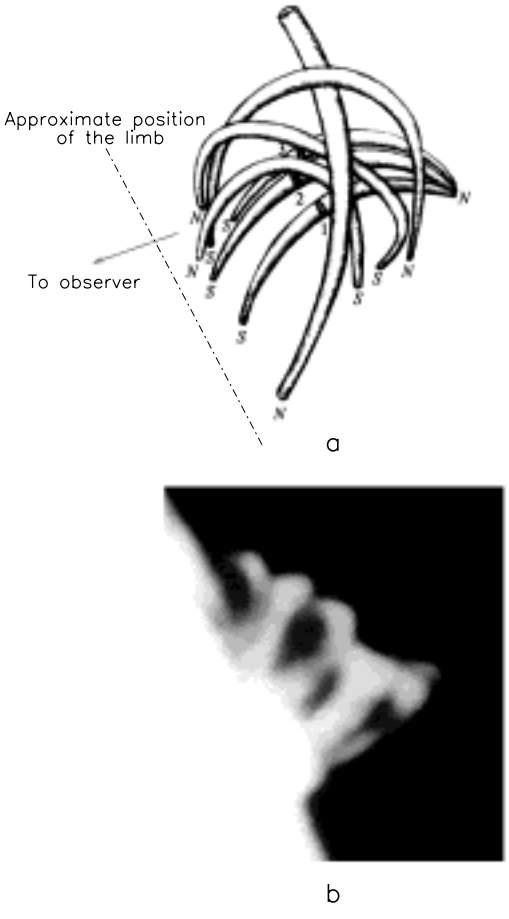


**Fig. 11.** Spatial configuration of the magnetic loop system. **a)** A sketch of possible spatial disposition of some foremost loops. The sources 1, 2, 3 are marked by digits. **b)** The photograph of the post flare loops made at Baikal Astronomical Observatory ($H_\alpha$, 06:05 UT) can help to obtain a picture of the loop system

peak of the burst. Different elementary flux tubes were subsequently reconnecting, and new microwave sources appeared. As a result, their sites shifted clockwise along the boundary between the oppositely polarized regions performing almost total revolution.

### *4.2. A scenario of the flare*

Relative motion of two oppositely-polarized regions before the flare reflected corresponding motion of the magnetic configuration. It suggests a shear motion at footpoints of interconnecting magnetic ropes which provided energy storage for the flare.

The flare began from below. Probably, the region of energy release in the beginning of the first stage was behind the limb, and we only saw its manifestations in tops of loops.

The steady exponential growth irrelative to changes of energy release sites suggests existence of some large-scale mechanisms forced to increase the rate of energy release in the first stage of the flare. Existence of the fine temporal structures shows that there was no efficient trapping of accelerated electrons.

To the end of the first stage, the trapping became efficient. Accelerated electrons were accumulated in the dome-like emitting region which rapidly grew. The time profile at 17 GHz became smoother. However, a fine (subsecond) temporal structure was observed to be emitted by a source appeared at 5.7 GHz above the dome-like one. It was located well above the soft X-ray kernel. The height of this source above the limb was close to the hard X-ray one's found by Nakajima & Metcalf (1995). So this upper

source can be classified as a "loop-top source" (Masuda 1994).

In the second stage, when the upper 5.7 GHz source disappeared, the dome-like source became uniformly weaker with decreasing of the number of accelerated electrons, but the gyrosynchrotron mechanism continued to provide the main contribution to the microwave emission.

In the third stage, two different processes of energy release also went on. Evidence of particle acceleration is given by the almost continuous series of sub-bursts observed at lower frequencies low in corona. Prolonged particle acceleration during the late phase of a flare was also revealed by Akimov et al. (1994). High in corona, a reconnection of the two interacting oppositely-polarized ropes continued, which was marked by the compact hot microwave source at the place of their closest contact located near the brightness centre in X-rays. Free-free emission from the post-flare loops seen in soft X-rays became the main component at high frequencies.

Ichimoto et al. (1993) analysed this flare in detail using X-ray and $H_\alpha$ data. Calculating the gas pressure and the magnetic one, they puzzled that the gas pressure exceeded the magnetic one, suggesting that the magnetic field was not strong enough to confine the hot plasma as rigidly as is commonly assumed (30 G). From the degree of polarization at 17 GHz, it follows that even the line-of-sight component of the magnetic field was $\geq 45$ G. So the magnetic configuration essentially differed from the potential one and could be sufficiently strong to balance the plasma pressure.

In summary, the observations of the present event seem to give evidence for the interaction of large-scale systems of multiple intercrossed flare loops during the whole development of the flare, and do not seem to be consistent with a merging of magnetic field lines at the tip of an inverse-Y-type field line configuration in long-duration events (LDEs) (see, e.g., Sturrock 1966; Kopp & Pneuman 1976; Tsuneta 1996). The flare of November 2, 1992 provides additional support to the existence of solar flares caused by interaction of loops (Kundu 1984; Machado et al. 1988; Hanaoka 1994; Hanaoka 1997; Inda-Koide et al. 1995; Shimuzu et al. 1994; Nishio et al. 1997).

## 5. Conclusion

1. It has appeared to be possible, to explain the main qualities of the flare within the framework of a closed configuration.
2. Studying how the pre-flare spatial structure developed has revealed the regions in which the line-of-sight component of the magnetic field had the opposite direction. The $LCP$-region was almost enveloped by the $RCP$ one. In the course of the flare, energy release sites appeared near the boundary between these regions.
3. Microwave sources of different origin were observed during the flare. The source with the spectral turnover frequency $< 10$ GHz corresponded to the energy release site and provided the main contribution into the total flux of the burst in the initial phase of the flare. When the burst reached its peak, the turnover frequency became two times more. Trapped electrons were responsible for the most part of the microwave emission during the impulsive phase.
4. The steady exponential growth of the brightness temperature and the flux of the microwave emission went on in the initial stage of the flare during an interval as long as almost 5 time constants. Sources essentially changed their spatial structure during this stage. So the development of the flare was conducted by some large-scale instability.
5. Sub-second pulses observed at 5.7 GHz during the impulsive phase were generated in the optically thin source which was observed in hard X-rays at a height of 34 $10^3$ km. The compact source of the sub-second pulses at 17 GHz was due to gyrosynchrotron emission of electrons with the energy of $1-2$ MeV. It had the size of 2 $10^3$ km and was located at a height of 15 $10^3$ km.
6. The energy release had not yet terminated during the post-flare stage till at least 06:00. Two regions of energy release can be followed in this stage: the upper one where the two opposite magnetic ropes contacted, and the lower one where the microwave sub-bursts of non-thermal origin occurred. Free-free emission from soft X-ray loops then became predominant.

*Acknowledgements.* A. Altyntsev and V. Grechnev use this opportunity to express their thanks for hospitality and help from the Nobeyama Solar Group during their work in Nobeyama Radio Observatory. We thank Dr. B. Lubyshev and Ms. G. Zubkova for a preliminary analysis of the SSRT data. We are greatly indebted to Dr. R. Ramaty for his kindness, to have made his code for calculation of gyrosynchrotron emission available for us. Part of this work was supported by the Russian projects of *RFFI* No. 96-02-16648, No. 97-02-16906 and *Astronomia*.

## References

Akimov V.V., Belov A.V., Chertok I.M., Kurt V.G., Leikov N.G., Magun A., Melnikov V.F., 1994, Proc. of Kofu Symposium, NRO report No. 360, July 1994, p. 371

Altyntsev A.T., Grechnev V.V., Kachev L.E., et al., 1994, A&A 287, 256

Altyntsev A.T., Grechnev V.V., Zubkova G.N., et al., 1995, A&A 303, 249

Altyntsev A.T., Grechnev V.V., Hanaoka Y., 1998, Solar Phys. 178, 575

Bai T., Ramaty R., 1976, Solar Phys. 49, 344

Benz A.O., 1986, Solar Phys. 104, 99

Feldman U., Seely J.F., Doschek G.A., Brown C.M., Phillips K.J.H., Lang J., 1995, ApJ 446, 860

Fujiki K., High spatial resolution imaging for the Nobeyama Radioheliograph and observations of weak activities prior to solar flares, 1997, Ph. D. thesis
Hanaoka Y., 1994, ApJ 420, L37
Hanaoka Y., 1997, Solar Phys. 173, 319
Ichimoto K., Sakurai T., Flare Telescope and Norikura Teams, Optical and X-ray observations of the X9 flare on 2nd Nov. 1992. Proc. of the Second Japan-China seminar on the Solar Physics, 1993 July 6-8, Sagamihara, Sakurai T. (eds.), G.Ai. NAO of Japan, Mitaka, Tokyo, 1993
Inda-Koide M., Sakai J., Koide S., Kosugi T., Sakao T., Shimizu T., 1995, PASJ 47, 323
Kopp R.A., Pneuman G.W., 1976, Solar Phys. 50, 85
Kundu M., 1984, Adv. Space Res. 4, 157
Machado M.E., Moore R.L., Hernandez A.M., Rovira M.G., Hagyard M.J., Smith J., 1988, ApJ 326, 425
Masuda S., 1994, Proc. of Kofu Symposium, NRO report No. 360, July 1994, p. 209
Nakajima H., Nishio M., Enome S., et al., 1994, Proc. IEEE 82, 705
Nakajima H., Metcalf T., 1995, Microwave and hard X-ray sources in two X-class limb flares. Proc. of High Energy Solar Physics, AIP Conf. Proc., p. 374
Nakajima H., et al., 1998 (in preparation)
Nishio M., Yaji K., Kosugi T., et al., 1997, ApJ 489, 976
Ramaty R., 1969, ApJ 158, 753
Ramaty R., et al., 1994, ApJ 436, 941
Simberova S., Karlicky M., Svestka Z., 1993, Solar Phys. 146, 343
Shimizu T., Tsuneta S., Acton L.W., et al., 1994, ApJ 422, 906
Smolkov G.Ya., Pistolkors A.A., Treskov T.A., et al., 1986, Astrophys. Space Sci. 119, 1
Sturrock P.A., 1966, Nat 211, 695
Tsuneta S., Acton L., Bruner M., et al., 1991, Solar Phys. 136, 37
Tsuneta S., 1996, ApJ 456, 840